Available online at www.sciencedirect.com

ScienceDirect

Procedia Manufacturing 51 (2020) 779–786

Procedia MANUFACTURING

www.elsevier.com/locate/procedia

30th International Conference on Flexible Automation and Intelligent Manufacturing (FAIM2021)
15-18 June 2021, Athens, Greece.

A residual stress measurement and numerical analysis round robin on a three-pass slot nickel-base repair weld

Vasileios Akrivos[a]*, Mike C Smith[a], Ondrej Muransky[b,c], Carsten Ohms[d], Anastasios Youtsos[e]

[a]*University of Manchester, Sackivlle Street, Manchester, UK, M13 9PL*
[b]*Australian Nuclear Science and Technology Organisation (ANSTO), Lucas Heights, NSW, Australia*
[c]*School of Mechanical and Manufacturing Engineering, UNSW Sydney, Sydney, Australia*
[d]*Joint Research Centre, European Commission, Westerduinweg 3, 1755 LE Petten, The Netherlands*
[e]*National Center of Scientific Research 'Demokritos' (Institute of Nuclear Technology & Radiation Protection), 153 10 Agia Paraskevi, Athens 60228, Greece*

* *Corresponding author. Tel.: +44 (0) 161 275 1916; fax: +44 (0) 161 275 1916.* E-mail address: *vasileios.akrivos@manchester.ac.uk*

Abstract

The activities within a European network to develop accurate experimental and numerical methods to assess residual stresses (RS) in structural weldments are reported. The NeT Task Group 6 or TG6 project examined an Alloy 600 plate containing a three-pass slot weld made with Alloy 82 consumables. A number of identical specimens were fabricated and detailed records of the manufacturing history were kept. Parallel RS measurement and simulation round robins were performed. RS were measured using neutron diffraction at five different instruments. The acquired database is large enough to generate reliable mean profiles, to identify clear outliers, and to establish the systematic uncertainty associated with this non-destructive technique. TG6 gives a valuable insight into the real-world variability of diffraction-based RS measurements, and forms a reliable foundation against which to benchmark other measurement methods. The mean profile of measured RS was used to validate the accuracy achieved by the network on the prediction of RS.

© 2020 The Authors. Published by Elsevier Ltd.
This is an open access article under the CC BY-NC-ND license (https://creativecommons.org/licenses/by-nc-nd/4.0/)
Peer-review under responsibility of the scientific committee of the FAIM 2021.

Keywords: Welding | Weld modelling | Residual stress measurement | Finite element modelling | Materials characterisation

1. Introduction

Residual stresses (RS) within a component can adversely affect its structural integrity, and reduce its lifetime as it becomes more susceptible to degradation mechanisms such as stress corrosion cracking, fatigue and creep [1]. Welding induced RS develop in and around the fusion zone due to shape misfits that arise from the thermal and mechanical load applied simultaneously during this manufacturing process. Weld RS in Ni alloys are important due to the susceptibility of such alloys to primary water stress corrosion cracking when used as part of dissimilar metal welds in pressurized water reactor primary circuits. These alloys are widely used in components as they offer similar thermal expansion coefficients to those of low alloy pressure vessel steel [2]. DMW is often used in nozzles, boiler tubes and penetrations of the reactor pressure vessel among others [3, 4]. The European Network NeT aims on Neutron Techniques Standardization for Structural Integrity (NeT). NeT was first established in 2002 with the mission to develop improved experimental and numerical methods and standards to reliably characterize the RS in structural welds. One of their most recent projects, called NeT- Task Group 6 or TG6, was started in early 2012 and examines the behavior of a specimen that includes a 3-pass slot weld in Alloy 600, made using the tungsten-inert-gas (TIG) welding process with an Alloy 82 filler. Previous benchmarks launched by the network

2351-9789 © 2020 The Authors. Published by Elsevier Ltd.
This is an open access article under the CC BY-NC-ND license (https://creativecommons.org/licenses/by-nc-nd/4.0/)
Peer-review under responsibility of the scientific committee of the FAIM 2021.
10.1016/j.promfg.2020.10.109

have proposed the best practices for accurate finite element (FE) analysis of welding to predict accurately the RS for a single weld bead [5] and for a multi pass weld deposited for AISI 316L(N) stainless steel [6].

Nomenclature

ANSTO	Australian Nuclear Science and Technology Organisation, Australia
CGHAZ	Coarse grain heat affected zone
DB	Doosan Babcock, United Kingdom
EC2	EC2 Modélisation, France
EdF	Électricité de France
FE	Finite Element
INR	Institute for Nuclear Research, Romania
IC	Imperial College, United Kingdom
ND	Neutron diffraction
NeT	European Network on Neutron Techniques Standardization for Structural Integrity
RBE	Robust Bayesian Estimation
RS	Residual stress
TIG	Tungsten inert gas
UoM	University of Manchester, United Kingdom
WCL	Weld centre line
WML	Weld middle length

2. The NeT TG6 Benchmark specimen

The TG6 specimen is a 3-pass slot weld in Alloy 600 Ni-Cr alloy (also referred to as Inconel 600), made using a TIG welding process with Alloy 82 filler. The chemical compositions as well as the mechanical properties of both the base and the filler materials are presented in Tables 1 and 2 respectively. An automated TIG welding machine was employed for welding the plates at the Électricité de France (EdF) laboratory in Chatou in France. Each TG6 specimen consists of a plate with a central groove filled with three superimposed weld beads. Figure 1 shows a typical TG6 specimen before and after welding, and the drawings with the dimensions of the plate and the slot size. The dimensions were carefully selected to allow for sufficient structural self-restraint of the plate while remaining thin enough to ensure that neutron diffraction measurements of RS are still feasible. Figure 1d illustrates planes D and B that correspond to the longitudinal plane along the weld center line (WCL) and the transverse plane at weld middle length (WML) respectively. Line BD is the line that extends through thickness of the plate at the junction of planes D and B. This line is of greatest interest for stress measurements and predictions because it passes through all three deposited weld beads as well as the cyclically hardened parent material. Because line BD is located at WML, it is considered that stable welding conditions have been reached.

3. Residual stress measurements round robin

A number of neutron diffraction (ND) RS measurements have been performed on one of the TG6 specimens, labelled as A5, using neutrons from both reactor and neutron spallation sources. Three orthogonal stress components were determined along several lines in the same plate. Measurements were also conducted on stress free pins extracted at representative locations from specimen A6 in accordance with Figure 2. Data analysis was informed by simple macroscopic studies (i.e. metallography) to distinguish the fusion zone as well as chemical composition studies such as electron micro-probe analysis that revealed dilution effects of each successive weld pool with melted parent material and re-melted weld beads.

There were three different approaches to analyze the neutron diffraction data. One was to use the data measured on the stress-free pins that were extracted from a second specimen, A6, which was welded using identical conditions and was subsequently cut into pieces (Figure 2). The second was based on position fitting where the laser scans of the plates after welding and the macrographs acquired were used to infer the exact measurement locations [7]. In particular, as seen in Figure 3 the profiles of the plate cut into pieces and the one used for ND RS measurements were compared. Transverse cross sections at WML and longitudinal cross sections at WCL were etched to reveal the fusion zone profiles. The RS measurements were modelled using the SSCANSS [8] software that allows to plan the experiment and simulate the measurements. The exact measurement locations of the gauge volume at each measurement point were then superimposed to the scanned profiles and the macrographs. This enabled the accurate estimation of a parent-weld fraction within the gauge volume at locations close to the fusion boundary. The small thickness of the plate (~12mm) allowed also the calculation of theoretical strain free value based on the assumption that the normal stress is almost zero. This approach was also justified by the results of preliminary FE simulations which were performed and presented in a previous study [9].

NeT TG6 also benefits from the fact that five series of measurements have been performed on the same specimen at diffractometers around the world. This allowed the calculation of a Robust Bayesian Estimate (RBE) of the mean by 'Duff Data' method individually for each stress component. The RBE mean was also implemented previously within NeT Task Group 4 or TG4 [10]. It is less susceptible to outliers, and thus a more reliable characterization of the RS distribution in the component could be made. The actual RBE uncertainties were also calculated by subtracting the systematic uncertainties form each data set and provided a more realistic approximation of the uncertainties associated with the RS measurements by ND. A detail description of the ND measurements, the analysis methodology and the RBE calculation are given in [11].

4. Residual stress simulation round robin

4.1. Thermal analyses

The thermal analysis was calibrated by each participant following a protocol [12] that provided all details about the welding process, as summarized in Table 3. A trial plate with three grooves was welded in the exact same way as the TG6 specimen, but the individual grooves were filled with one, two and three pass welds, respectively, and then used for characterization purposes as seen in Figure 4a. A strain relief EDM contour cut was initially performed in the transverse

Table 1. Summary of chemical composition (certificate) for Alloy 600 parent plate and Alloy 82 filler wire (welding of TG6 specimens).

Material	C	Si	Mn	Cr	Ni	S	Nb	Ti	Fe
Alloy 600 (wt. %)	0.07	0.12	0.48	15.54	74.35	0.001	0.10	0.006	9.33
Alloy 82 (wt. %)	0.009	0.08	3.25	20.8	72.7	0.001	2.6	0.319	0.59

Table 2. Summary of material properties (certificate) for Alloy 600 parent plate and Alloy 82 filler wire (welding of TG6 specimens).

Material	Yield **Stress** 0.2% (MPa)	Ultimate Tensile Strength (MPa)	Elongation (%)
Alloy 600 **(**wt. %**)**	401	706	40.4
All**oy** 82 **(**wt. %**)**	380	620	35

Table 3. Summary of Welding Procedure for TG6 Specimen [13]

Parameter	Pass 1	Pass 2	Pass 3
Plate Material	Alloy 600	Alloy 600	Alloy 600
Welding Process	GTAW	GTAW	GTAW
Filler Wire	Alloy 82	Alloy 82	Alloy 82
Wire Diameter	1 mm	1 mm	1 mm
Arc Polarity	DC Electrode (-)	DC Electrode (-)	DC Electrode (-)
Shielding Gas	Argon	Argon	Argon
Tungsten Electrode	2% Lantane	2% Lantane	2% Lantane
Arc Length	4 mm	4 mm	4 mm
Electrode Diameter	2.4 mm	2.4 mm	2.4 mm
Gas Cup ID	8 mm	8 mm	8 mm
Gas Flow Rate	10-12 l/min	10-12 l/min	10-12 l/min
Gas Pre-Purge	Start - 5 s	Start - 5 s	Start - 5 s
Arc On Start	Start + 0 s	Start + 0 s	Start + 0 s
Starting Current	0 A	0 A	0 A
Start of Ramp Up Start	Start + 0 s	Start + 0 s	Start + 0 s
End of Ramp Up Start	Start + 1s	Start + 1s	Start + 1s
Pulsing Frequency	1 Hz	1 Hz	1 Hz
Peak Welding Current	240 A	240 A	240 A
B/G Welding Current	200 A	200 A	200 A
Arc Voltage	10.3-11.2V	12.7-14.0V	11.5-13.0V
Start of Wire Feed	Start + 2.5s	Start + 2.5s	Start + 2.6s
Peak Wire Feed Speed	1.7 m/mn	1.7 m/mn	1.7 m/mn
B/G Wire Feed Speed	1.5 m/mn	1.5 m/mn	1.5 m/mn
Start of Travel	Start + 4.5s	Start + 4.5s	Start + 4.6s
Travel Speed	70.0 mm/min	70.0 mm/min	70.0 mm/min
Weaving	None	None	None
End of Travel	End + 0s	End + 0s	End + 0s
Start of Ramp Down	End + 0s	End + 0s	End + 0s
End of Wire Feed	End + 1.5s	End + 1.5s	End + 1.5s
End of Ramp Down	End + 6.5s	End + 6.5s	End + 6.5s
Final Current	5 – 10 A	5 – 10 A	5 – 10 A
Inter-pass Temperature	20 °C +/- 10 °C	50 – 60 °C	50 – 60 °C

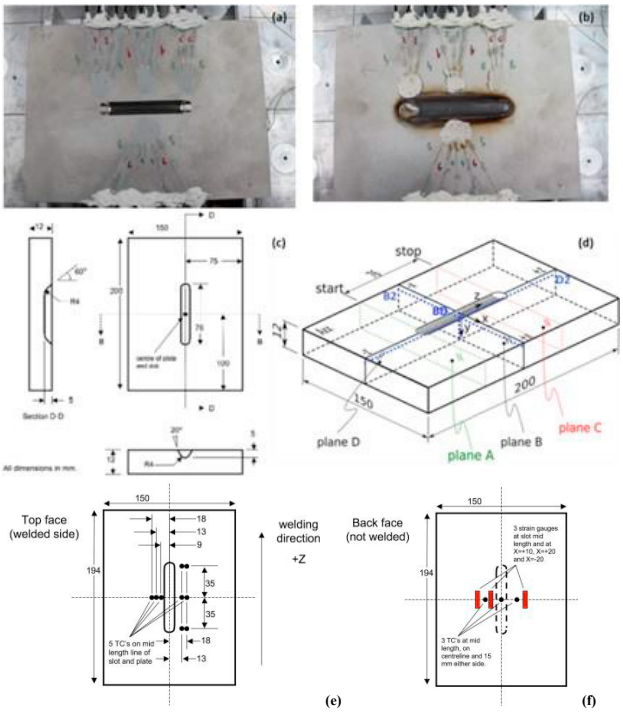

Fig. 1. Specimen A6 instrumented with thermocouples (a) before and (b) after welding. (c) Schematic representation of the TG6 specimen showing the dimensions of the plate and the machined slot and (d) the co-ordinate system. Start and stop refer to the start and stop ends of the weld. The nominal thermocouple positions on the (e) top and (f) bottom surface of the specimen [13].

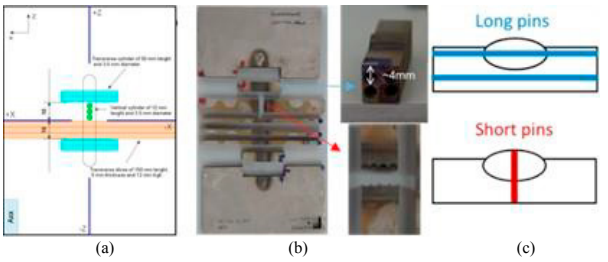

Fig. 2. (a) Cutting plan for extraction of reference specimens from specimen A6 [14], (b) specimen A6 after the extraction of the stress free pins and slices and (c) the locations of the extracted pins used as stress free reference samples.

plane at WML to study the evolution of RS after each pass (Figure 4a, b). Slices were then extracted to be used for characterization. As seen in Figure 4c the different weld beads can be seen with the naked eye. The slices were then polished and etched for optical metallography (Figure 4d). The macrographs revealed the fusion zone and the distinct different weld beads as well as a ~1mm distinct coarse grain heat affected zone (CGHAZ) surrounding the fusion boundary. The inferred fusion profiles along with the recorded thermocouple histories were used to calibrate the heat source shape and size. Some participants used a weld heat source modelling tool called FEAT-WMT [15] that allows the accurate definition of a welding heat source. It makes use of a steady state 3D moving mesh solution to simulate a moving heat source. Most of the participants used a simple ellipsoid shape moving heat source with a Gaussian distribution in a 3D-half model (Figure 5) aiming to match the temperature histories of the far-field thermocouples at WML and the fusion zone shape and size. The exact weld bead lengths at each pass were defined based on the torch traverse lengths and the welding parameters histories (i.e. voltage, current as a function of time), which can be found in Table 3. The dwells as well as the power ramps were also considered at start and stop ends respectively for each pass.

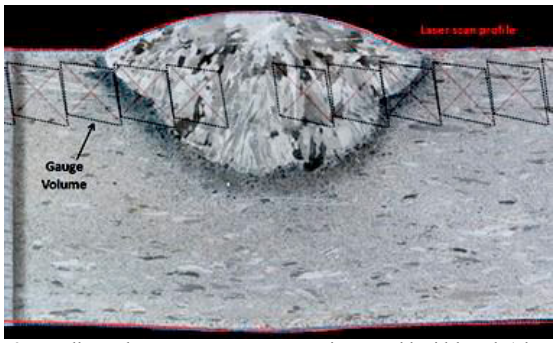

Fig. 3. Metallography on transverse cross section at weld mid-length (plane B) superimposed on laser scans of two specimens and the theoretical gauge volume at neutron diffraction measurements using the SSCANSS software.

Radiative and convective heat exchanges of the specimen with the environment have been considered by all participants in the simulations, the coefficient of convection h was 8W m^{-1} K^{-1}, the Stefan- Boltzmann constant σ was $5.67*10^{-14}$ W m^{-2} K^{-4} and the material emissivity ε was 0.7. The external temperature was set to 20°C. The temperature dependent thermo-physical properties used were the same for both parent and weld metal and were used by all participants [12]. The methodology followed to calibrate the thermal analysis was based on the outcomes of the NeT-Task Group 1 or TG1 round robin [5, 16] and has also been included into the weld modelling guidelines in the R6 structural integrity assessment procedure [17]. The accuracy targets were to remain within ±20% of the measured fused area for each weld bead and within ±10% deviation of a root mean square error between the predicted and measured temperature rises of the combined far field thermocouples located at WML. The latter has been described before in the NeT TG4 benchmark [6].

An example of the thermocouple responses from nine TG6 specimens compared with the predicted ones for a single pass is given in Figures 6a for the thermocouples located the bottom surface at WML of the plate and Figure 6b at the top surface of the plate. The predicted responses are generally in very good agreement with the measured ones. The measured and predicted fusion zones at WML are presented in Figure 6c. The predicted fusion zone shape and size at each pass is presented using the 1400°C isotherm.

4.2. Mechanical analyses

The TG6 specimen was left unclamped and free to distort during welding. Any mechanical restraint was due to inhomogeneous temperature fields occurring within the specimen during welding and cooling which leads to

incompatibilities of the strains between the hot fusion and adjacent heat affected zones and the cooler surrounding material. Almost all the mechanical simulations considered a 3D half model (INR used a quarter model approach) and a symmetry plane in the longitudinal direction along the WCL. Two nodes located at the top surface corners of the specimen along the WCL were also used to eliminate any motion of rigid bodies. One node was fixed along the normal direction and the other one both along normal and longitudinal directions. Temperature dependent elastic mechanical properties namely Young's modulus (E), Poisson ratio (v) and thermal expansion (α) were provided by the protocol to all participants and used for both the parent and the weld materials [12]. The mechanical analyses employed the Chaboche mixed isotropic-kinematic hardening [18] model available in different FE packages (i.e. Abaqus, ANSYS and Code_Aster). The Chaboche mixed hardening formulation, which is described elsewhere [19], is designed to simulate cyclic inelastic strains by allowing the yield surface both to expand or contract through isotropic hardening and translate through kinematic hardening.

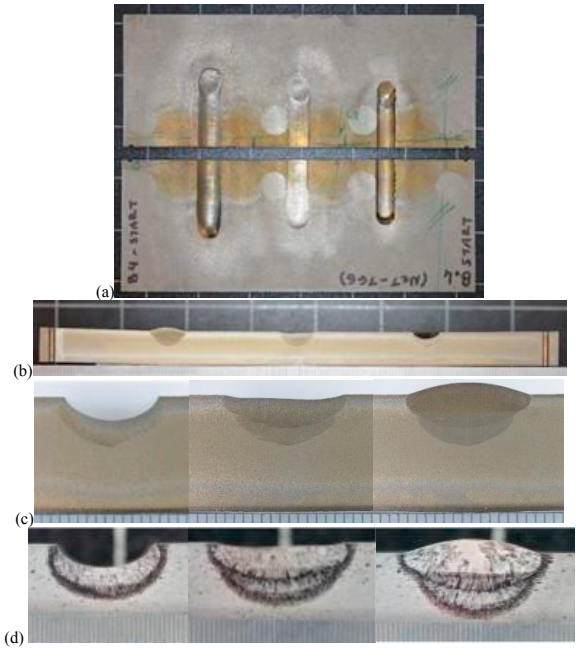

Fig. 4. (a) The trial three-slot specimen filled with a single, two and three weld passes after the performed EDM contour cut and (b) a view of the transverse-normal plane after cutting. (c) The three slices extracted from one half and (d) the macrographs acquired after chemical etching of the samples.

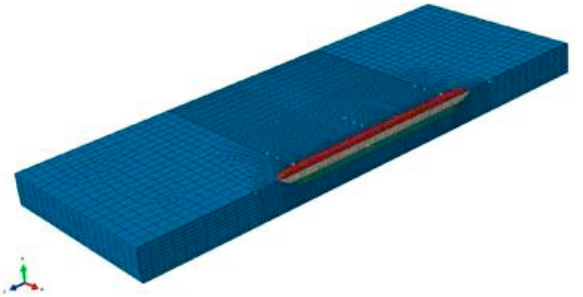

Fig. 5. Typical finite element half-model of TG6 specimen.

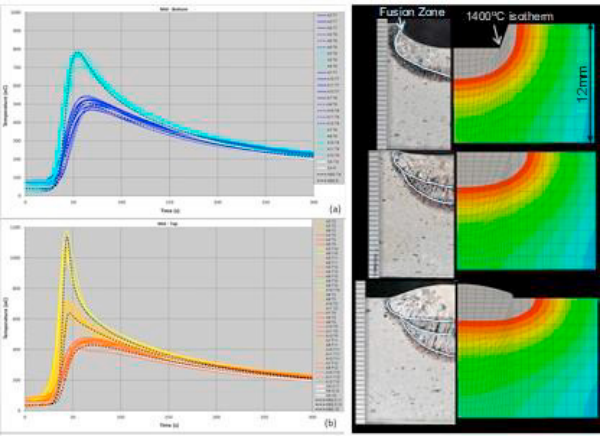

Fig. 6. Predicted and measured temperatures along plane B during first pass at thermocouples located at (a) mid-bottom, (b) mid-top. (c) The macrographs and predicted fusion profiles comparison.

To utilize this constitutive behavior, there are minimum of five parameters that need to be fitted using an isothermal uniaxial cyclic test. Aside from yield strength σ|0 one needs to fit two parameters per back-stress tensor (i.e. C_1–γ_1, C_2–γ_2) to describe kinematic hardening and two parameters (Q_{inf}, b) for the isotropic hardening component. All participants used two back-stress tensors (INR used also a third tensor) to describe kinematic hardening, hence a total of seven parameters were fitted for the conventional Chaboche model at each temperature. These were fitted by UoM either to reproduce the first monotonic response or the second reloading into tension of the isothermal cyclic tests. A study provides details about the Chaboche parameters and their behaviour and has shown that this has a profound effect on the predicted RS after welding simulation [20]. However, the available cyclic data from isothermal uniaxial low cycle fatigue tests done at 1.5%TSR for alloy 600 and alloy 182 (the manual metal arc welding filler surrogate) were also circulated in a simulation protocol [12] giving the liberty to any participant who wanted to refit the Chaboche parameters or use a different constitutive behavior. For instance, EC2 used the data to fit an elasto-plastic mixed hardening Prager model. UoM performed a supplementary test matrix using a spare plate of alloy 600 and a fabricated alloy 82 weld pad. The tests were made at 2.5%TSR for temperatures between 20-600°C and the results of this study are presented in [21]. The Chaboche parameters derived from these tests were used by UoM for their second contribution to the weld modelling campaign. Details of the FE simulations conducted by different NeT participants are provided in Table 4.

5. Discussion

Contour maps of a set of predicted transverse and longitudinal stresses (UoM-B) across planes D and B at WCL and WML, respectively, are presented in Figure 7. The stresses predicted are lower in the fusion zone compared to those in the base metal owing to the low yield strength and cyclic hardening rate of the weld metal. The transverse stresses are tensile in the vicinity of the weld balanced by compressive stresses in the plate (Figure 7a). The longitudinal stresses are even higher in the weld and drop into compression further away from the weld toward the edges of the plate (Figure 7b). A higher tensile stress

field is seen in the stop position area for both stress components. Figure 8 encloses the stress predictions provided by the participants against the RBE of measurements for each stress component separately for line BD. The latter has been identified as the most important line of measurement points as it goes through several zones that have been subjected into different thermo-mechanical histories, namely the different weld beads, the heat affected zone and the cyclically hardened parent zone. The RBE mean is plotted in yellow and the error bars are the actual RBE uncertainties after subtracting the systematic uncertainty from each individual set [9].

Table 4. Summary of the details of the different weld modelling attempts by all NeT participants

Organisation	FE package	Elements	Constitutive behaviour	Annealing	Heat Source
EC2-A	Code Aster	~30000 Hexahedral 1st order	Chaboche - 1.5%TSR monotonic fit parent/weld	800-950 ºC Linear two stage	Moving (triangular shaped)
EC2-B	Code Aster	~10000 Hexahedral 2nd order	Prager 1.5%TSR	800-950 ºC Linear two stage	Moving (triangular shaped)
INR	ANSYS (3D 1/4 model)	25470 Quadratic hexahedral	Chaboche - 1.5%TSR monotonic fit parent/weld	1100 ºC Single stage	Fixed (block dump)
IC-A	Abaqus	69380 Linear	Chaboche - 1.5%TSR monotonic fit parent/weld	1050 ºC Single stage	Moving (Goldak elllipsoid)
IC-B	Abaqus	69380 Linear	Chaboche - 1.5%TSR monotonic/cycle 2 fit parent/weld	1050 ºC Single stage	Moving (Goldak elllipsoid)
ANSTO-A	Abaqus	40722 Quadratic hexahedral	Chaboche - 1.5%TSR monotonic fit parent/weld	1050 ºC Single stage	Moving (Goldak elllipsoid) FEAT-WMT
ANSTO-B	Abaqus	40722 Quadratic hexahedral	Chaboche - 1.5%TSR monotonic/cycle 2 fit parent/weld	1050 ºC Single stage	Moving (Goldak elllipsoid) FEAT-WMT
UoM-A	Abaqus	40722 Quadratic hexahedral	Chaboche – 1.5%TSR monotonic fit parent Cycle-2 fit weld	1050 ºC Single stage	Moving (Goldak elllipsoid) FEAT-WMT
UoM-B	Abaqus	40722 Quadratic hexahedral	Chaboche - 2.5%TSR monotonic fit parent Cycle-2 fit weld	1050 ºC Single stage	Moving (Goldak elllipsoid) FEAT-WMT
DB	Abaqus	100862 Quadratic hexahedral	Chaboche – 1.5%TSR monotonic fit parent/weld	1050 ºC Single stage	Moving (Goldak elllipsoid)

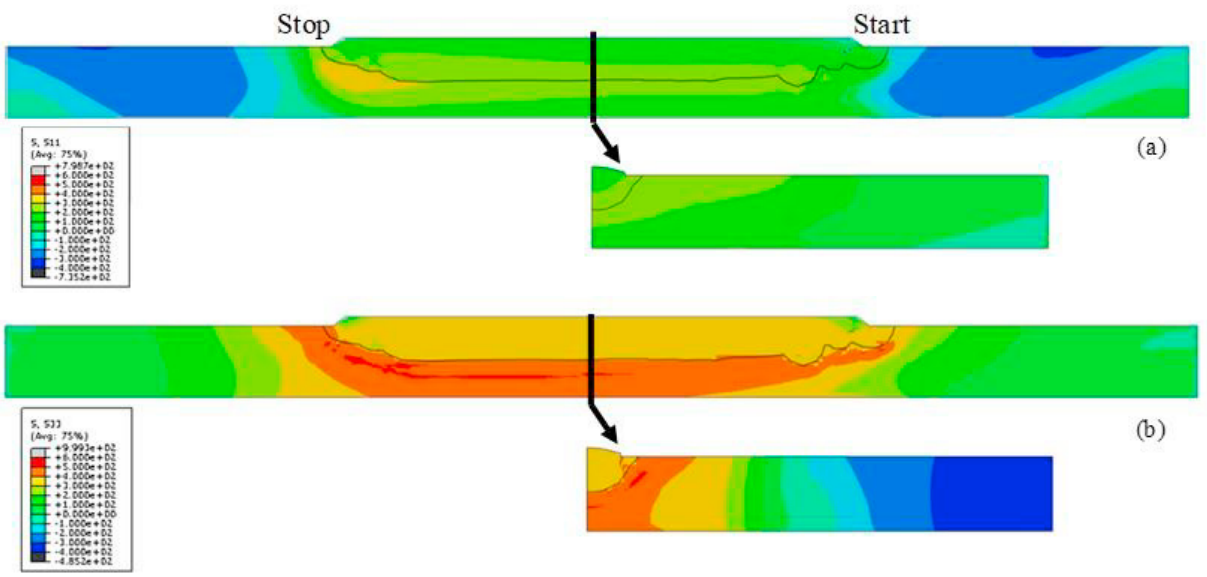

Fig. 7. Predicted (a) transverse and (b) longitudinal stresses on planes D and B from UoM-B simulation.

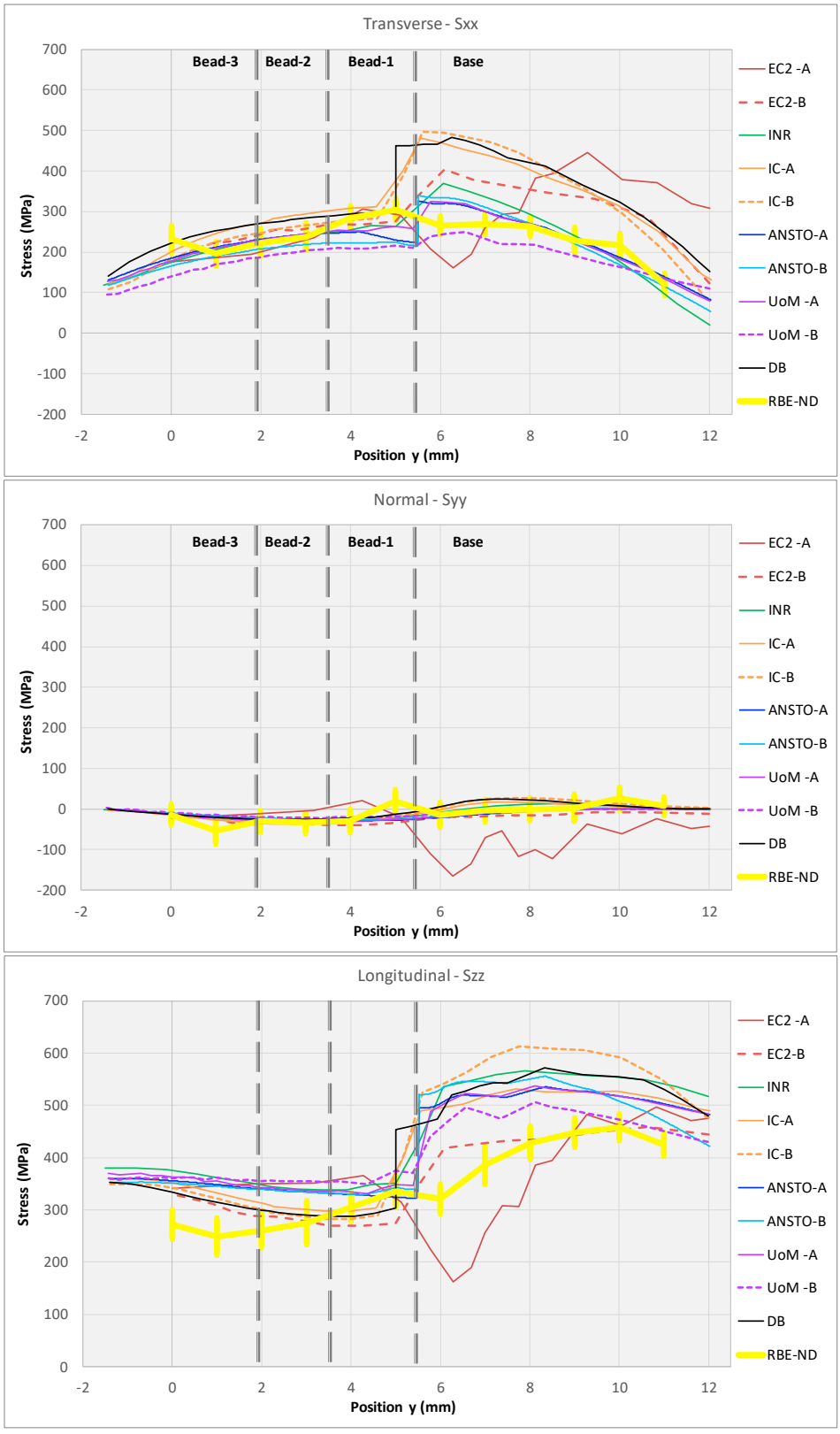

Fig. 8. Comparison of the predicted (a) transverse, (b) normal and (c) longitudinal stresses on line BD from the different welding simulations performed with the neutron diffraction-based Bayesian mean.

Both longitudinal and transverse stress components are tensile throughout BD line. The transverse stress peaks around the first pass of weld metal decreasing to almost zero at the bottom surface of the plate (Figure 8a) whereas the longitudinal stresses are lower in the fusion zone than in the base metal which is attributed to the different mechanical properties of weld and parent metals (Figure 8c). However, the two stress components are fairly similar in distribution and amount within the fusion zone. Most simulations seem to predict well the transverse stresses both in the fusion zone and the parent plate. They also predict reasonably low normal stresses (Figure 8b). Interestingly, there is a large scatter on the predictions of the longitudinal stress profile. Almost all simulations predict higher longitudinal stress in the fusion zone where the second and the third pass have been laid which indicated that the just deposited material is much softer than it was expected. Moreover, all simulations significantly overestimate the stresses in the parent material and in particular in the HAZ. This is believed to arise from the 1mm thick CGHAZ which is much softer than the rest of the parent material, and this shows the need for a more sophisticated approach to annealing/recovery effects.

6. Concluding Remarks

The NeT-TG6 has generated a sufficient amount of mechanical testing data, information on the material behavior inferred from simple and more advanced characterization techniques and a number of RS measurements and welding simulation predictions so far. However, to date the accurate RS prediction on the TG6 benchmark still remains a challenge. The full scope of the project has never been entirely described and published. The project is still ongoing and more simulations are yet to be delivered by NeT participants.

Acknowledgements

The project was funded by the EPSRC Industrial CASE Award Nº1502808, and the EPSRC Fellowship in Manufacturing, “A whole-life approach to the development of high integrity welding technologies for Generation IV fast reactors”, EP/L015013/1. The authors wish to acknowledge the substantial in kind contributions made by Dr Viorel Deaconu (INR), Dr Lionel Depradeux (EC2), Dr Priyesh Kapadia (Imperial College) and Dr Tamba Dauda (Doosan Babcock) for delivering FE simulations as well as all the participants within the NeT network for performing the non-destructive measurements. The authors would also like to acknowledge the support from EdF in France who co-sponsored this research and fabricated the weldments.

References

[1] Bouchard, P.J., Residual Stresses in Lifetime and Structural Integrity Assessment. Encyclopedia of Materials: Science and Technology (Second Edition), 2001: p. 8134–8142.

[2] Scott, P.M. and C. Benhamou, An overview of recent observations and interpretations of IGSCC in nickel base alloys in PWR primary water, in Tenth international conference on environmental degradation of materials in nuclear power systems – water reactors. August 2001, TMS (The Minerals, Metals & Materials Society): , Lake Tahoe, Nevada.

[3] Ballinger, R.G., Light water reactors: materials of construction and their performance, in International conference on plant materials degradation - Application to the stress corrosion cracking of Ni-base alloys. ,November 2008: EDF R&D centre of Les Renardieres, Moret–Sur–Loing, France.

[4] Clement, R., PWRs systems and operation, in International conference on plant materials degradation - Application to the stress corrosion cracking of Ni base alloys. , November 2008: , EDF R&D centre of Les Renardieres, Moret Sur Loing, France.

[5] Smith, M.C., et al., A review of the NeT Task Group 1 residual stress measurement and analysis round robin on a single weld bead-on-plate specimen. International Journal Pressure Vessel and Piping 2014. 120-121(0): p. 93-140.

[6] Smith, M.C., et al., The NeT Task Group 4 residual stress measurement and analysis round robin on a three-pass slot-welded plate specimen. International Journal of Pressure Vessels and Piping, 2018. 164: p. 3-21.

[7] Akrivos, V. and M.C. Smith, Material Characterization on the Nickel-Based Alloy 600/82 NeT-TG6 Benchmark Weldments, in ASME Pressure Vessels and Piping Conference, Boston, PVP2019-94017. 2019. p. V06BT06A062.

[8] James, J., et al., A virtual laboratory for neutron and synchrotron strain scanning. Physica B, 2004. 350(1–3): p. E743–6.

[9] Smith, M.C., et al., The NeT-Task Group 6 Weld Residual Stress Measurement and Simulation Round Robin in Alloy 600/82, in Proceedings of the ASME 2016 Pressure Vessels and Piping Conference PVP 2016. 2016, ASME PVP 2016: Vancouver, British Columbia, Canada.

[10] Wimpory, R.C., et al., Statistical analysis of residual stress determinations using neutron diffraction. International Journal of Pressure Vessels and Piping, 2009. 86(1): p. 48-62.

[11] Akrivos, V., et al., On the neutron diffraction measurements of weld residual stresses in three-pass slot-weld (Alloy 600/82) and the assessment of the measurement uncertainty (Submitted fro publication). Journal of Applied Crystallography, 2020.

[12] Smith, M.C., NeT TG6 finite element simulation protocol, Issue 1 for Phase 1 simulations. January 2016.

[13] Smith, M.C., et al., NeT-TG6 The Manufacture of a Three-Pass Slot Weld Specimen in Inconel 600 Nickel/Chromium Alloy. June 2014.

[14] Ohms, C., et al., NeT-Task Group 6: Three-Pass Slot Weld Specimen in Inconel Nickel/Chromium Alloy Protocol for the Destructive and Non-Destructive Determination of Residual Stress in a Three-Pass Slot Weld Specimen in Inconel Nickel/Chromium Alloy. June 2015.

[15] FEAT, User Guide, Version 3.15.0. Feat Plus Limited, 2013.

[16] Smith, M.C. and A.C. Smith, NeT bead-on-plate round robin: comparison of transient thermal predictions and measurements. International Journal of Pressure Vessels and Piping, 2009. 86: p. 96-109.

[17] R6, Assessment of the integrity of structures containing defects, EDF Energy (2015).

[18] Chaboche, J.L., Constitutive equations for cyclic plasticity and cyclic viscoplasticity. International Journal of Plasticity, 1989. 5: p. 247–302.

[19] Smith, M.C., et al., Optimisation of mixed hardening material constitutive models for weld residual stress simulation using the NeT Task Group 1 single bead on plate benchmark problem. 2009: ASME PVP 2009, Prague, PVP2009- 77158.

[20] Muránsky, O., et al. (2012). "The effect of plasticity theory on predicted residual stress fields in numerical weld analyses." Computational Materials Science 54: 125-134.

[21] Akrivos, V. and M.C. Smith, The thermo-mechanical behaviour of the Alloy 600 and Alloy 82 materials, in Proceedings of the ASME 2018 Pressure Vessels and Piping Conference PVP 2018. 2018: ASME PVP 2018: Prague, Czech Republic.